


Minimal Quantization Model in Pilot-Wave Hydrodynamics

Austin M. Blitstein¹, Rodolfo R. Rosales², and Pedro J. Sáenz^{1,*}

¹*Department of Mathematics, University of North Carolina, Chapel Hill, North Carolina 27599, USA*

²*Department of Mathematics, Massachusetts Institute of Technology, Cambridge, Massachusetts 02139, USA*

 (Received 25 June 2023; revised 6 October 2023; accepted 31 January 2024; published 8 March 2024)

Investigating how classical systems may manifest dynamics analogous to those of quantum systems is a broad subject of fundamental interest. Walking droplets, which self-propel through a resonant interaction with their own wave field, provide a unique macroscopic realization of wave-particle duality that exhibits behaviors previously thought exclusive to quantum particles. Despite significant efforts, elucidating the precise origin and form of the wave-mediated forces responsible for the walker’s quantumlike behavior remained elusive. Here, we demonstrate that, owing to wave interference, the force responsible for orbital quantization originates from waves excited near stationary points on the walker’s past trajectory. Moreover, we derive a minimal model with the essential ingredients to capture quantized orbital dynamics, including quasiperiodic and chaotic orbits. Notably, this minimal model provides an explicit distinction between local forces, which account for the walker’s preferred speed and wave-induced added mass, and spatiotemporal nonlocal forces responsible for quantization. The quantization mechanism revealed here is generic, and will thus play a role in other hydrodynamic quantum analogs.

DOI: [10.1103/PhysRevLett.132.104003](https://doi.org/10.1103/PhysRevLett.132.104003)

Fluid dynamics has a history of introducing influential, cross-disciplinary concepts, like solitons [1,2], as well as offering valuable insights into otherwise relatively inaccessible physical phenomena, including the Aharonov-Bohm effect [3], superradiance [4,5], black holes [6], and the Casimir effect [7]. Hydrodynamic quantum analogs (HQAs) focus on investigating the extent to which pilot-wave hydrodynamics [8] may exhibit behaviors previously deemed peculiar to the quantum realm [9]. Multiple classical pilot-wave systems are being developed [10–13], motivated by the discovery of droplets that spontaneously walk along the surface of a vibrating fluid bath [Fig. 1(a)] [14]. Acting as a self-propelled wave source guided by its own “pilot” wave field [8,15], the droplet excites at each bounce a spatiotemporally decaying Faraday wave [16], with wavelength λ_F , whose longevity and spatial extent increase with the bath’s driving acceleration γ [17]. When γ exceeds a critical walking threshold, γ_W , the droplet starts to land on the slope of the wave field generated at prior bounces, experiencing a wave-induced horizontal force at the point of impact that propels it forward [18,19]. A key feature of the system is its “memory,” quantified by the characteristic wave decay time [17]. As γ increases toward the Faraday threshold [20], the waves excited at each bounce decay more slowly and so the droplet’s past significantly influences its evolution. By virtue of the coupling with their underlying wave field, walking droplets, or “walkers,” exhibit numerous HQAs, including orbital quantization [21–23], single particle diffraction and interference [24–28], tunneling [29–31], wavelike statistics [32,33] and superposition of states

[34,35], Friedel oscillations [36], collective spin order [37], and double quantization in a harmonic well [38–40].

A crucial unresolved question is elucidating the precise origin and form of the spatiotemporal nonlocal forces that underlie the walkers’ quantization. We provide an answer within the context of the HQA of orbital quantization [21–23], which leverages the mathematical equivalence between the Lorentz force $q(\mathbf{v} \times \mathbf{B})$, acting on a charge q moving with velocity \mathbf{v} in a magnetic field \mathbf{B} , and the Coriolis force $2m(\mathbf{v} \times \mathbf{\Omega})$, acting on a mass m moving with velocity \mathbf{v} in a frame rotating at constant angular velocity $\mathbf{\Omega}$. Classically, a charge in a magnetic field and a mass in a rotating frame lead to circular orbits, whose radius varies continuously with the magnitude of the force field $r(B) = mv/qB$ and $r(\Omega) = v/2\Omega$, respectively. In contrast, a quantum particle in a magnetic field exhibits quantized orbits in which the allowed radii take values in a discrete set $r_n \approx (n + 1/2)\lambda_{dB}/2\pi$ ($n = 0, 1, 2, \dots$), where λ_{dB} is the particle’s de Broglie wavelength [41]. At sufficiently high memory, an analogous orbital quantization occurs for a walking droplet in a rotating frame. Owing to the influence of its pilot-wave field, the droplet’s orbital radius is equivalently discretized with preferred radii $r_n \approx (n + 3/4)\lambda_F/2$ ($n = 0, 1, 2, \dots$) [21,23].

Progress has been made toward understanding the walker’s orbital quantization [21,23,33,40,42–46]. Fort *et al.* [21] proposed the notion of a “virtual walker” diametrically opposite the walker’s position to interpret their experimental observations. Oza *et al.* [23] later showed that the discrete orbital radii observed in

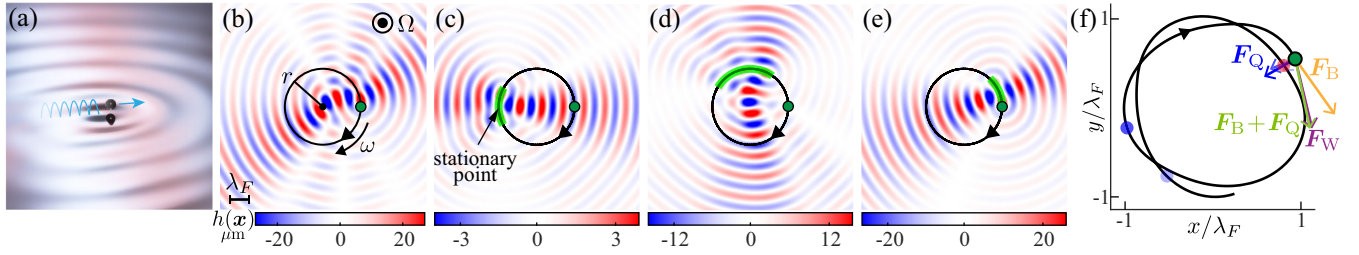


FIG. 1. (a) Oblique view of a walking droplet, or walker, self-propelled by its wave field as seen in experiments. (b)–(e) Top view of the wave field of a walker (green disk) traveling clockwise along a circular orbit of radius r with orbital frequency ω in a bath rotating counterclockwise with angular frequency Ω . The full wave field in (b) is generated by the waves excited by the drop at each bounce along its past trajectory. We can thus decompose the wave field [shown in (b)] according to wave contributions [shown in (c)–(e)] produced by the walker along different portions of the past trajectory (highlighted in bright green). Waves excited in the vicinity of stationary points interfere constructively at the droplet’s location (c), causing orbital quantization, while those produced elsewhere interfere destructively at the droplet’s location (d), except for the waves excited in the walker’s recent past (e). (f) Quasicircular orbit illustrating the emergence of stationary points at different locations. The pilot-wave force F_W is approximated by the sum of nonlocal forces F_Q emanating from stationary points (blue) and a local boost force F_B . Stationary points near the droplet (red) may be neglected on account of the wave force being small. (Photo copyright: Abel J. Abraham).

experiments [21,22] correspond to stable circular solutions of the walker’s equation of motion [19]. Liu *et al.* [46] recently rationalized the stability of circular solutions in terms of the mean wave field produced by the drop.

We here demonstrate that the walker’s orbital quantization is caused by exponentially small wave-mediated forces arising from waves excited at stationary points of the distance function to the droplet’s past locations [Fig. 1(c)]. We calculate analytically the quantizing force resulting from constructive interference, which gives rise to a sinusoidal potential in the radial direction that restricts the allowed radii. Waves excited at other past locations interfere destructively at the droplet’s position [Fig. 1(d)], and may thus be safely neglected. By adding the quantizing force to the so-called “boost” force [47], which accounts for the wave force due to the recent past [Fig. 1(e)], we develop a minimal quantization model that captures the walker’s orbital dynamics [Fig. 1(f)].

Stroboscopic model.—Consider the dynamics of a walker in a fluid bath subjected simultaneously to vertical oscillations with forcing acceleration $\gamma \sin(2\pi ft)$, and constant rotation around the vertical axis with angular frequency Ω . The centrifugal force on the droplet is balanced by the lateral force resulting from bouncing on the parabolic surface of the bath, and so both effects may be excluded [21,22]. In the frame of reference rotating with the bath, the dimensionless equation of motion for the droplet position $\mathbf{x}(t)$ is then

$$\kappa \mathbf{x}'' + \mathbf{x}' = \mathbf{x}' \times \boldsymbol{\Omega} + \mathbf{F}_W, \quad (1)$$

where the characteristic scales for space, time, and bath rotation rate are $1/k_F = \lambda_F/2\pi$, T_M , and $D/2m$, respectively. Here, $\kappa = m/DT_M$ is the dimensionless mass, D is the drag coefficient accounting for viscous dissipation

during flight and impact with the bath, $T_M = T_d/(1 - \gamma/\gamma_F)$ is the wave-decay time, or memory time, T_d is the wave-decay time in the absence of vibration [18], and γ_F is the Faraday threshold, beyond which standing waves spontaneously arise in the bath [20].

The walker is propelled by the horizontal wave force F_W , exerted when the droplet lands on the slope of the underlying wave field [19]. At each bounce, the droplet excites a zeroth-order Bessel function with wave number k_F and decay time T_M [18]. By noting that the droplet bouncing occurs on a timescale $2/f$, much shorter than that of the horizontal walking dynamics T_M , Oza *et al.* [19] proposed to approximate the droplet as a continuous wave source. The wave force may thus be computed by an integral over the gradient of the waves produced in the walker’s past,

$$\mathbf{F}_W = \beta \int_0^\infty J_1(|\mathbf{d}(s)|) \frac{\mathbf{d}(s)}{|\mathbf{d}(s)|} e^{-s} ds, \quad (2)$$

where $\beta = mgA \sin(\phi) k_F^2 f T_M^2 / 2D$ is a dimensionless force coefficient, A is the wave amplitude, ϕ is the impact phase, and $\mathbf{d}(s) = \mathbf{x}(t) - \mathbf{x}(t-s)$ [19]. The integro-differential equation of motion (1) and (2) is the so-called “stroboscopic” model [19].

Minimal quantization model (MQM).—We compute an approximation to F_W that captures explicitly the quantizing force on the droplet due to the waves excited in the vicinity of stationary points, which interfere constructively at the droplet’s location. Stationary points are extrema of the distance function to the droplet’s past positions, $d(s) = |\mathbf{d}(s)|$, satisfying $d'(s_j) = 0$. To proceed, we make the assumptions that the orbits are large and quasicircular, and only distant stationary points $d(s_j) \gg 1$ are significant. The condition on the distance allows us to approximate the

Bessel kernel as $J_1(d(s)) \approx \sqrt{2/\pi d(s)} \sin[d(s) - \pi/4]$, and so transform (2) into an expression amenable to the stationary phase method [48,49]. The wave force may thus be approximated by $\mathbf{F}_W \approx \mathbf{F}_Q + \mathbf{F}_B$, where

$$\mathbf{F}_Q = \text{Im} \left[\beta e^{-i\frac{\pi}{4}} \sum_j \int_{s_j - \delta_j}^{s_j + \delta_j} \sqrt{\frac{2}{\pi d(s)}} \frac{d(s)}{d(s)} e^{id(s)-s} ds \right] \quad (3)$$

is the contribution from the stationary points, and \mathbf{F}_B is the contribution from the end of the integration interval, which corresponds to the walker's most recent path. Here, δ_j satisfies $0 < \delta_j = O(1/\sqrt{d(s_j)}) \ll 1$ and denotes the width of the region that leads to constructive interference at the droplet's current location. The sum is over all stationary points with $d''(s_j) < 0$ [local maxima of $d(s)$], which tend to be diametrically opposite the droplet in a quasicircular orbit [Fig. 1(f)]. Stationary points with $d''(s_j) > 0$ [local minima of $d(s)$], which tend to be near the droplet, may be safely neglected since $J_1(d) \rightarrow 0$ as $d \rightarrow 0$.

Relevant points to the stationary phase method, or extrema of the imaginary phase $id(s)$, coincide with the physical stationary points on the orbits. To improve the approximation at high memory, we use the more general complex phase $\Psi(s) = id(s) - s$, and apply the saddle-point method [48,49], which picks up the contribution from saddle points in the complex plane z_j , satisfying $\Psi'(z_j) = 0$. Notably, we only have access to the orbits $\mathbf{x}(t)$ for real t . To circumvent this, we assume that the saddle points z_j are close to the stationary points s_j , which allows us to complexify $d(s)$ by expanding near the stationary points, $d(z) \approx d(s_j) + \frac{1}{2}d''(s_j)(z - s_j)^2$. At this point all that remains is to perform the saddle-point calculation (see Supplemental Material [50]), which yields

$$\mathbf{F}_Q = \sum_j [A_{r,j} \cos \varphi_j + A_{t,j} \sin \varphi_j] e^{-s_j}, \quad (4)$$

where $\varphi_j = d(s_j) - \frac{1}{2}K_j$, and the force components are

$$\begin{aligned} A_{r,j} &= -2\beta B_j \left(d(s_j) + \frac{1}{2}K_j^2 \mathbf{x}''(t - s_j) \right), \\ A_{t,j} &= 2\beta B_j K_j \mathbf{x}'(t - s_j), \end{aligned} \quad (5)$$

where $A_{r,j}$ is a predominantly radial component, and $A_{t,j}$ is a purely tangential component. Here, $K_j = |d''(s_j)|^{-1}$, and $B_j = (d(s_j) + \frac{1}{2}K_j)^{-3/2} \sqrt{K_j}$.

To complete a minimal model for the walker's orbital dynamics, we complement (4) with the end point contribution to the wave force due to the recent history [Fig. 1(e)] in accordance with the standard practice of stationary phase-type approximations. This contribution was computed by Bush *et al.* [47] in the weak acceleration limit, $\mathbf{x}' = \mathbf{x}'(\epsilon t)$, for $\epsilon \ll 1$,

$$\mathbf{F}_B = C(|\mathbf{x}'|)\mathbf{x}' + \kappa \left[\mathbf{x}'' - \frac{d}{dt}(\gamma_B(|\mathbf{x}'|)\mathbf{x}') \right], \quad (6)$$

where $C(u) = (\beta/u^2)(1-p)$, and $\gamma_B(u) = 1 + \frac{1}{2}(\beta/\kappa)p^3$, with $p = 1/\sqrt{1+u^2}$. The first term in (6) combined with the friction term in (1) gives a Rayleigh-like drag term that selects a preferred walking speed, $u_0 = (-1 + 2\beta - \sqrt{1+4\beta})^{1/2}/\sqrt{2}$. The second term is the inertial force due to the wave-induced added mass $(\gamma_B - 1)\kappa$, which tends to enlarge the orbits. This wave force is referred to as the boost contribution, as γ_B resembles the Lorentz boost factor for a relativistic particle [47].

By approximating the stroboscopic wave force (2) to leading order, $\mathbf{F}_W \approx \mathbf{F}_B + \mathbf{F}_Q$, we thus obtain the MQM,

$$\kappa \mathbf{x}'' + \mathbf{x}' = \mathbf{x}' \times \boldsymbol{\Omega} + \mathbf{F}_B + \mathbf{F}_Q, \quad (7)$$

which contains the minimal ingredients necessary to capture the walker's quantized orbital dynamics. Notably, the MQM provides a clear distinction between the local force \mathbf{F}_B , which depends on variables at the walker's current position, and spatiotemporal nonlocal forces \mathbf{F}_Q , which originate at past locations and are responsible for quantization. Note that the MQM may be seen as an example of "asymptotics beyond all orders" [51] since \mathbf{F}_Q is exponentially smaller than \mathbf{F}_B , yet is solely responsible for the walker's orbital quantization. We discuss limitations of our asymptotic approximations in Supplemental Material [50].

Mechanism for orbital quantization.—The wave-mediated quantizing force (4) makes the mechanism responsible for orbital quantization apparent. Any generic curved trajectory has stationary points, which generate a beam [Fig. 1(c)] that tends to drive the walker into a quasicircular orbit. In this quasicircular orbit [Fig. 1(f)], the walker and relevant stationary points are approximately diametrically opposite. The tangential component of (4), $A_{t,j} \sin \varphi_j$, weakly perturbs the walker's orbital speed from u_0 due to being relatively small compared to the boost force that acts in the same direction. The radial component of (4), $A_{r,j} \cos \varphi_j$, generates an effective potential that pushes the walker toward the minima of $\sin \varphi_j$, which correspond to the preferred radii r_n observed in experiments. For circular orbits $\varphi_j \approx 2r$, which leads to $r_n \approx (n + 3/4)\lambda_F/2$ ($n = 0, 1, 2, \dots$).

Circular orbits.—To investigate quantitatively the circular orbits admitted by the MQM, we look for solutions to (7) of the form $\mathbf{x}(t) = r(\cos \omega t, \sin \omega t)$, which results in the following system of algebraic equations,

$$\begin{aligned} -\kappa \gamma_B(u) r \omega^2 &= \boldsymbol{\Omega} u + N(\omega) e^{-\pi/|\omega|} A_r \cos \varphi, \\ [1 - C(u)] u &= N(\omega) e^{-\pi/|\omega|} A_t \sin \varphi, \end{aligned} \quad (8)$$

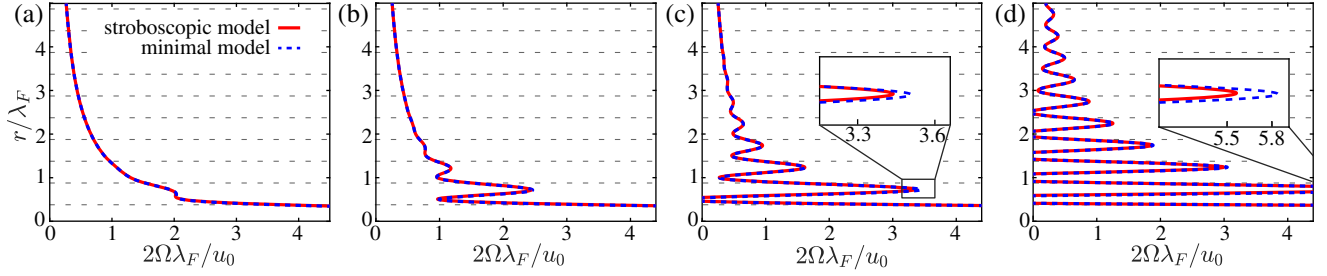


FIG. 2. Orbital solutions to the MQM and stroboscopic model. Memory increases from left to right, with (a) $\gamma/\gamma_F = 0.922$, (b) $\gamma/\gamma_F = 0.954$, (c) $\gamma/\gamma_F = 0.971$, and (d) $\gamma/\gamma_F = 0.985$. Excellent agreement is observed except for a few small discrepancies shown with insets in (c),(d), which have a negligible effect in the orbital quantization. Black dashed lines correspond to $r_n = (n + 3/4)\lambda_F/2$.

where r , ω , and $u = r\omega$ are the walker's orbital radius, frequency, and velocity, respectively. Note that all local maxima of $d(s)$ are diametrically opposite the walker for circular orbits, thus $A_{r,j}$, $A_{t,j}$, and φ_j are the same for each term in (4), namely $A_r = -2\beta(u^2 + 1)(u^2 + 1/2)^{-3/2}$, $A_t = -2\beta u(u^2 + 1/2)^{-3/2}$, and $\varphi = 2r(1 - 1/2u^2)$. The factor $N(\omega) = 1/(1 - e^{-2\pi/|\omega|})$, which arises from summing over all stationary points, provides a measure of how many points are important. For the remainder of this Letter, κ and β are chosen according to experiments with 20 cSt silicon oil, vibrating frequency $f = 80$ Hz, and drop radius 0.4 mm [52].

We solve the system (8) numerically for (r, ω, Ω) and compare in Fig. 2 the resulting orbital radii $r(\Omega)$ with those from the equivalent analysis performed with the stroboscopic model [23]. Excellent agreement is observed across memories γ/γ_F , even for the smallest radii where the asymptotic analysis used to derive the MQM is expected to break down. As the memory increases, minor discrepancies arise for small orbits [Figs. 2(c) and 2(d)]. We

observe analogous quantitative agreement for the orbital frequency $\omega(\Omega)$.

Orbital dynamics and stability.—To demonstrate that the MQM leads to the same stable orbits as the full stroboscopic model, we simulate numerically (7) and examine the emergent dynamics. Following [52], for a given memory γ/γ_F , we initialize the walker along a circular orbit with radius r , orbital frequency ω , and bath frequency Ω defined by (8). We truncate the sum over stationary points in the quantizing force once subsequent partial sums agree within 0.1%.

A typical stable circular orbit produced by the MQM is presented in Fig. 3(a). Even though the orbit is relatively small, $r/\lambda_F = O(1)$, the MQM and stroboscopic forces are nearly identical (Supplemental Material, Video 1 [50]). Not all circular orbit solutions are stable; walker's initialized in orbits larger or smaller than the preferred orbits will either jump-up or jump-down in radius to reach the closest stable orbit [Figs. 3(b) and 3(c)]. Moreover, as the memory increases, circular solutions become unstable to lateral oscillations leading to a range of exotic orbits [52]. Most of the previously reported exotic orbits are also captured by the MQM [Figs. 3(d)–3(f)], for which the MQM and stroboscopic forces coincide in an average sense (Supplemental Material, Video 2 [50]). We were unable to

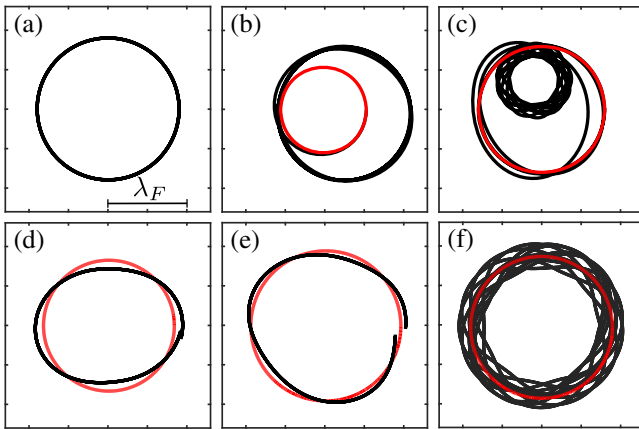


FIG. 3. Among previously known orbits, the MQM captures (a) circular $(r/\lambda_F, \gamma/\gamma_F) = (0.9, 0.95)$, (b) jump-up $(0.55, 0.94)$, (c) jump-down $(0.8, 0.97)$, (d) 2ω -wobble $(0.85, 0.955)$, (e) 3ω -wobble $(0.94, 0.9745)$, and (f) quasiperiodic orbits $(0.893, 0.966)$. Walker's were initialized in circular orbits of radius r (red).

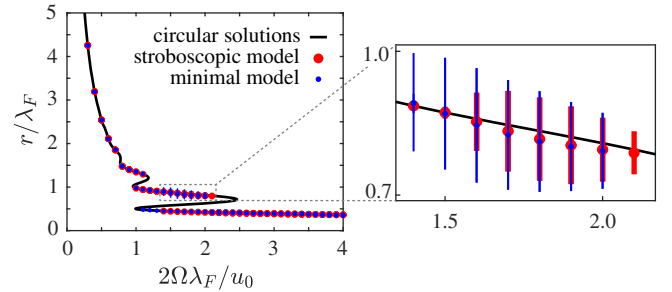


FIG. 4. Dependence of mean orbital radius r on bath rotation frequency for walkers evolved with the MQM and stroboscopic model at $\gamma/\gamma_F = 0.954$. Error bars indicate the maximum radial deviation from the mean. The black curve denotes all circular orbit solutions, as in Fig. 2(b). Both models predict the same plateaus.

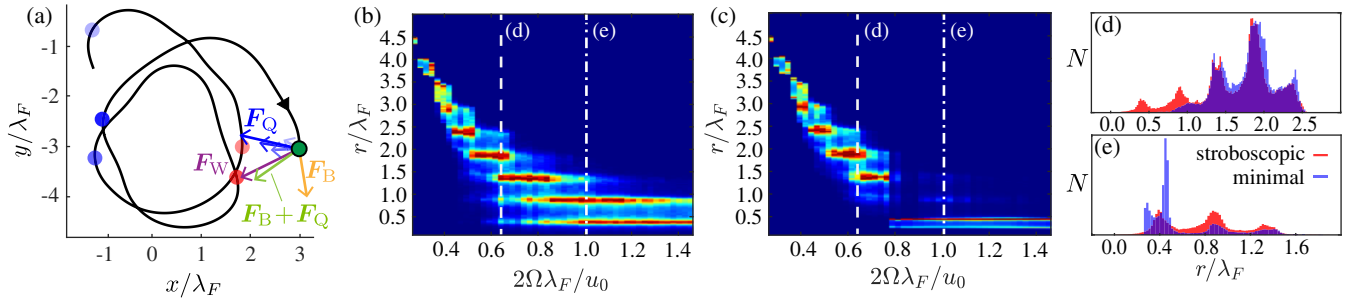


FIG. 5. Statistical quantization at $\gamma/\gamma_F = 0.980$. (a) Forces on the droplet for a chaotic trajectory generated by the MQM due to an intricate interplay between stationary points. Radial statistics for the (b) stroboscopic model, and (c) MQM. Each vertical line is a histogram of the radius of curvature for fixed bath rotation frequency, as seen in (d) and (e). Good agreement is found for low bath rotation frequency (d).

find the relatively infrequent orbits that either wobble and spontaneously leap to a new location, or are quasiperiodic with high curvature segments where the asymptotics of the MQM break down. Notably, the MQM allows us to rationalize wobbling orbits as radial oscillations in the beamlike potential created by the stationary points [Fig. 1(c)]. Stable orbits produced by the minimal and stroboscopic models are compared across orbital radii and bath rotation rates at intermediate memory (Fig. 4). Both models agree well; only minor differences are observed in the amplitude of the radial oscillations of some wobbling orbits.

Chaotic orbits.—In the high memory regime, the walker’s motion becomes chaotic [Fig. 5(a)], yet orbital quantization emerges in a statistical sense [22,52]. A histogram of the instantaneous radius of curvature reveals a chaotic switching between preferred radii coinciding with those observed for circular orbits [Fig. 5(b)]. The MQM captures well the statistical quantization for low bath rotation frequency, where larger orbits are more frequent [Fig. 5(c)]. In this regime, the route to chaos may thus be rationalized through the appearance of numerous stationary points that exert forces on the walker in different directions, destabilizing the circular orbit solutions and so inducing transitions between the preferred radii (Supplemental Material, Video 3 [50]). The disagreement for high bath rotation frequency is a consequence of small orbits at high memory being in a regime inaccessible to our asymptotic approximations (see Supplemental Material [50]).

Discussion.—Through an asymptotic reduction of the stroboscopic model [19], we have identified the precise origin and form of the spatiotemporal nonlocal forces responsible for the walker’s orbital quantization. We demonstrated that the quantizing force arises from constructive interference of waves excited by the droplet at stationary points along its past trajectory. This insight has allowed us to derive a minimal quantization model that explicitly distinguishes between spatiotemporal local and nonlocal forces, the latter being responsible for quantization. Our work thus reveals how wave-mediated nonlocal

effects may lead to quantumlike behaviors in HQAs [9]. The generic nature of the quantizing mechanism described here invites a reexamination of other analogs with comparable orbital dynamics [38–40] and walkers departing from straight-line motion [53–57]. Moreover, the concept of stationary points readily extends to problems involving the interaction of multiple walkers [37,56–58], where additional stationary points emerge in the distance functions from each walker to the past locations of all other walkers, and entirely new pilot-wave systems inspired by walking droplets, including those realized with stratified flows [10], canoes [11], capillary surfers [12], and acoustically forced bubbles [13].

P. J. S. acknowledges support through an Alfred P. Sloan Research Fellowship and the National Science Foundation CAREER Award No. CBET-2144180.

*saenz@unc.edu

- [1] N. J. Zabusky and M. D. Kruskal, *Phys. Rev. Lett.* **15**, 240 (1965).
- [2] C. S. Gardner, J. M. Greene, M. D. Kruskal, and R. M. Miura, *Phys. Rev. Lett.* **19**, 1095 (1967).
- [3] M. V. Berry, R. G. Chambers, M. D. Large, C. Upstill, and J. C. Walmsley, *Eur. J. Phys.* **1**, 154 (1980).
- [4] K. Papatryfonos, M. Ruelle, C. Bourdiol, A. Nachbin, J. W. M. Bush, and M. Labousse, *Commun. Phys.* **5**, 142 (2022).
- [5] V. Frumkin, J. W. M. Bush, and K. Papatryfonos, *Phys. Rev. Lett.* **130**, 064002 (2023).
- [6] W. G. Unruh, *Phys. Rev. Lett.* **46**, 1351 (1981).
- [7] B. C. Denardo, J. J. Puda, and A. Larraza, *Am. J. Phys.* **77**, 1095 (2009).
- [8] J. W. M. Bush, *Annu. Rev. Fluid Mech.* **47**, 269 (2015).
- [9] J. W. M. Bush and A. U. Oza, *Rep. Prog. Phys.* **84**, 017001 (2020).
- [10] P. Le Gal, B. Castillo Morales, S. Hernandez-Zapata, and G. Ruiz Chavarria, *J. Fluid Mech.* **931**, A14 (2022).
- [11] G. P. Benham, O. Devauchelle, S. W. Morris, and J. A. Neufeld, *Phys. Rev. Fluids* **7**, 074804 (2022).

- [12] I. Ho, G. Pucci, A. U. Oza, and D. M. Harris, *Phys. Rev. Fluids* **8**, L112001 (2023).
- [13] A. Roux, J.-P. Martischang, and M. Baudoin, *J. Fluid Mech.* **952**, A22 (2022).
- [14] Y. Couder, S. Protière, E. Fort, and A. Boudaoud, *Nature (London)* **437**, 208 (2005).
- [15] S. Protière, A. Boudaoud, and Y. Couder, *J. Fluid Mech.* **554**, 85 (2006).
- [16] M. Faraday, *Phil. Trans. R. Soc. London* **121**, 299 (1831).
- [17] A. Eddi, E. Sultan, J. Moukhtar, E. Fort, M. Rossi, and Y. Couder, *J. Fluid Mech.* **674**, 433 (2011).
- [18] J. Moláček and J. W. M. Bush, *J. Fluid Mech.* **727**, 612 (2013).
- [19] A. U. Oza, R. R. Rosales, and J. W. M. Bush, *J. Fluid Mech.* **737**, 552 (2013).
- [20] K. Kumar and L. Tuckerman, *J. Fluid Mech.* **279**, 49 (1994).
- [21] E. Fort, A. Eddi, A. Boudaoud, J. Moukhtar, and Y. Couder, *Proc. Natl. Acad. Sci. U.S.A.* **107**, 17515 (2010).
- [22] D. M. Harris and J. W. M. Bush, *J. Fluid Mech.* **739**, 444 (2013).
- [23] A. U. Oza, D. M. Harris, R. R. Rosales, and J. W. M. Bush, *J. Fluid Mech.* **744**, 404 (2014).
- [24] Y. Couder and E. Fort, *Phys. Rev. Lett.* **97**, 154101 (2006).
- [25] A. Andersen, J. Madsen, C. Reichelt, S. Rosenlund Ahl, B. Lautrup, C. Ellegaard, M. T. Levinsen, and T. Bohr, *Phys. Rev. E* **92**, 013006 (2015).
- [26] T. Bohr, A. Andersen, and B. Lautrup, in *Recent Advances in Fluid Dynamics with Environmental Applications* (Springer, New York, 2016), pp. 335–349, 10.1007/978-3-319-27965-7_25.
- [27] M. Rode, J. Madsen, and A. Andersen, *Phys. Rev. Fluids* **4**, 104801 (2019).
- [28] C. Ellegaard and M. T. Levinsen, *Phys. Rev. E* **102**, 023115 (2020).
- [29] A. Eddi, E. Fort, F. Moisy, and Y. Couder, *Phys. Rev. Lett.* **102**, 240401 (2009).
- [30] A. Nachbin, P. A. Milewski, and J. W. M. Bush, *Phys. Rev. Fluids* **2**, 034801 (2017).
- [31] L. Tadrist, T. Gilet, P. Schlagheck, and J. W. M. Bush, *Phys. Rev. E* **102**, 013104 (2020).
- [32] D. M. Harris, J. Moukhtar, E. Fort, Y. Couder, and J. W. M. Bush, *Phys. Rev. E* **88**, 011001(R) (2013).
- [33] M. Durey, P. A. Milewski, and Z. Wang, *J. Fluid Mech.* **891**, A3 (2020).
- [34] P. J. Sáenz, T. Cristea-Platon, and J. W. M. Bush, *Nat. Phys.* **14**, 315 (2017).
- [35] T. Cristea-Platon, P. J. Sáenz, and J. W. M. Bush, *Chaos* **28**, 096116 (2018).
- [36] P. J. Sáenz, T. Cristea-Platon, and J. W. M. Bush, *Sci. Adv.* **6**, eaay9234 (2020).
- [37] P. J. Sáenz, G. Pucci, S. E. Turton, A. Goujon, R. R. Rosales, J. Dunkel, and J. W. M. Bush, *Nature (London)* **596**, 58 (2021).
- [38] S. Perrard, M. Labousse, M. Miskin, E. Fort, and Y. Couder, *Nat. Commun.* **5**, 3219 (2014).
- [39] K. M. Kurianski, A. U. Oza, and J. W. M. Bush, *Phys. Rev. Fluids* **2**, 113602 (2017).
- [40] M. Durey and P. A. Milewski, *J. Fluid Mech.* **821**, 296 (2017).
- [41] L. D. Landau and E. M. Lifshitz, *Quantum Mechanics: Non Relativistic Theory* (Pergamon Press, New York, 1994).
- [42] M. Labousse, A. U. Oza, S. Perrard, and J. W. M. Bush, *Phys. Rev. E* **93**, 033122 (2016).
- [43] M. Labousse, S. Perrard, Y. Couder, and E. Fort, *New J. Phys.* **16**, 113027 (2014).
- [44] M. Labousse, S. Perrard, Y. Couder, and E. Fort, *Phys. Rev. E* **94**, 042224 (2016).
- [45] A. U. Oza, R. R. Rosales, and J. W. M. Bush, *Chaos* **28**, 096106 (2018).
- [46] N. Liu, M. Durey, and J. W. M. Bush, *J. Fluid Mech.* **973**, A4 (2023).
- [47] J. W. M. Bush, A. U. Oza, and J. Moláček, *J. Fluid Mech.* **755**, R7 (2014).
- [48] C. M. Bender and S. A. Orszag, *Advanced Mathematical Methods for Scientists and Engineers* (MacGraw-Hill, New York, 1978).
- [49] E. T. Copson, *Asymptotic Expansions* (Cambridge University Press, Cambridge, 1965).
- [50] See Supplemental Material at <http://link.aps.org/supplemental/10.1103/PhysRevLett.132.104003> for the derivation of the quantizing force, a discussion of the limitations of our asymptotic approximations, and movies of the orbits predicted by the MQM.
- [51] H. Segur, S. Tanveer, and H. Levine, *Asymptotics beyond All Orders* (Springer, New York, 2012).
- [52] A. U. Oza, Ø. Wind-Willassen, D. M. Harris, R. R. Rosales, and J. W. M. Bush, *Phys. Fluids* **26**, 082101 (2014).
- [53] G. Pucci, P. J. Sáenz, L. M. Faria, and J. W. M. Bush, *J. Fluid Mech.* **804**, R3 (2016).
- [54] G. Pucci, D. Harris, L. Faria, and J. W. M. Bush, *J. Fluid Mech.* **835**, 1136 (2018).
- [55] S. Protière, S. Bohn, and Y. Couder, *Phys. Rev. E* **78**, 036204 (2008).
- [56] A. U. Oza, E. Siéfert, D. M. Harris, J. Moláček, and J. W. M. Bush, *Phys. Rev. Fluids* **2**, 053601 (2017).
- [57] J. Arbeláiz, A. U. Oza, and J. W. M. Bush, *Phys. Rev. Fluids* **3**, 013604 (2018).
- [58] M. M. P. Couchman, S. E. Turton, and J. W. M. Bush, *J. Fluid Mech.* **871**, 212 (2019).